ELSEVIER

Thermochimica Acta 308 (1998) 3–22

thermochimica acta

Interaction between water and hydrophilic polymers[1]

Hyoe Hatakeyama[a,*], Tatsuko Hatakeyama[2,b]

[a] *Fukui Institute of Technology, 3-6-3, Gakuen, Fukui 910, Japan*
[b] *National Institute of Materials and Chemical Research, 1-1, Higashi, Tsukuba, Ibaraki 305, Japan*

Received 15 October 1996; received in revised form 9 January 1997; accepted 18 August 1997

Abstract

Various natural and synthetic polymers with hydrophilic groups, such as hydroxyl, carboxyl and carbonyl groups, have either a strong or weak interaction with water. Thermal properties of polymers and water are both markedly influenced through this interaction. The first-order phase transition of water fractions closely associated with the polymer matrix is usually impossible to observe. Such fractions are called non-freezing water. Less closely associated water fractions exhibit melting/crystallization, showing considerable supercooling and significantly smaller enthalpy than that of bulk water. These water fractions are referred to as freezing bound water. The sum of the freezing bound and non-freezing water fractions is the bound water content. Water, whose melting/crystallization temperature and enthalpy are not significantly different from those of normal (bulk) water, is designated as freezing water. Bound water in the water–insoluble hydrophilic polymers, such as cellulose, lignin and poly(hydroxystyrene) derivatives, breaks hydrogen bonding between the hydroxyl groups of the polymers. The bound water content depends on the chemical and high-order structure of each polymer. Aqueous solutions of water-soluble polyelectrolytes, such as hyaluronic acid, gellan gum, xanthan gum and poly(vinyl alcohol) form gels above a threshold concentration. In the above gels, water mostly exists as the freezing bound water, playing an important role in the junction zone formation. It has also been observed that various kinds of polysaccharide polyelectrolytes with mono- and divalent cations, and other polyelectrolytes, such as polystyrene sulfonate, form thermotropic/lyotropic liquid crystals in the water content, ranging from 0.5 to ca. 3.0 g of water/g of polymer. © 1998 Published by Elsevier Science B.V.

1. General aspects of the water–hydrophilic polymer interaction

Hydrated polymer systems have been widely investigated owing to the effect of water on the performance of commercial polymers and the crucial role played by water–polymer interactions in biological processes. In the presence of excess water, a polymer may become swollen, exhibiting major changes in mechanical and chemical properties. Water can plasticize the polymer matrix or form stable bridges through hydrogen bonding, resulting in an anti-plasticizing effect. The behaviour of water can be transformed in the presence of a polymer, depending on the degree of chemical or physical association between the water and polymer phases.

Water, whose melting/crystallization temperature and enthalpy of melting/crystallization are not significantly different from those of normal (bulk) water, is called freezing water. Those water species exhibit-

*Corresponding author. Tel.: +81-776-22-8111; fax: +81-776-29-7891.

[1]Presented at the 14th IUPAC Conference on Chemical Thermodynamics, held in Osaka, Japan, 15–30 August, 1996.

[2]Tel. and fax: +81-298-54-6250.

PII S0040-6031(97)00325-0

ing large differences in transition enthalpies and temperatures, or those for which no phase transition can be observed calorimetrically, are referred to as bound water. It is frequently impossible to observe crystallization exotherms or melting endotherms for water fractions very closely associated with the polymer matrix. Such fractions are called non-freezing water. Less closely associated water fractions do exhibit melting/crystallization peaks, but often considerable supercooling is observed and the area of the peaks on both, the heating and cooling cycles is significantly smaller than that of bulk water. These water fractions are referred to as freezing bound water. The sum of the freezing bound and non-freezing water fractions is the bound water content.

2. Experimental

2.1. Bound water content determination by DSC

2.1.1. Determination of dry sample mass

DSC is commonly used to determine the proportions of the various water fractions present in hydrated polymers. Hermetically-sealed-type sample vessels are commonly used. If aluminium sample vessels are to be used, they should be placed in an autoclave with a small amount of pure water at 373 K for several hours to eliminate the formation of aluminium hydroxide on the surface of the sample vessel [1].

All polymers contain a small amount of water which is absorbed during synthesis, processing or storage. This kind of closely associated water remains in the polymer matrix, even after heating the polymer to 373 K under reduced pressure. It is important to establish the amount of this water fractions in order to know the total amount of water present in the sample after hydration. To determine this intrinsic water content, the sample should be weighed as accurately as possible, noting that the sample will absorb water from the atmosphere during weighing. A microbalance with sensitivity of the order of μg is necessary.

The sample vessel is pierced quickly, placed in the DSC at room temperature and heated at 10 K/min. An endothermic deviation in the sample baseline due to the vaporization of water is observed. The heat of vaporization of water is high (2257 J/g). The presence of a very small amount of water can be detected by this procedure. The sample is heated until no deviation in the sample baseline is observed. The dried sample is then quickly reweighed and the intrinsic water content determined.

2.1.2. Determination of freezing, freezing bound and non-freezing water

The uniformly hydrated sample is placed in the DSC at the room temperature (ca. 50°C) and cooled at 5–10 K/min to 150 K. The sample is held at 150 K for 15 min, and reheated to the room temperature at the same rate. The observed temperature and number of crystallization exotherms depend on the nature of the polymers and the water content (W_c). In this paper, the following definition will be used:

$$\text{Water content}(W_c) = (\text{g of water})/(\text{g of dry polymer}),\ (\text{g/g})$$

As shown in Fig. 1, the first-order phase transition is not detected until a critical amount of water is added to a polymer (curve I, Fig. 1). The amount of water is defined as non-freezing water content (W_{nf}). The maximum W_{nf} depends on hydrophilicity of polymers. When W_c in the polymers exceeds a critical amount (the maximum amount of W_{nf}), a small peak (peak II) is observed at a temperature lower than the crystal-

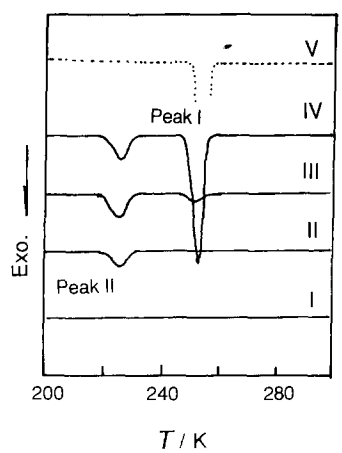

Fig. 1. Schematic DSC cooling curves of water sorbed on hydrophilic polymers: (———) – adsorbed water; (· · ·) – bulk water; I – non-freezing bound water (W_{nf}); II – W_{nf}+freezing bound water (W_{fb}); III, IV – W_{nf}+W_{fb}+free water (W_f); and V – bulk water.

lization peak of bulk water. The amount of water is categorized as freezing bound water content (W_{fb}). Free water (W_f) is shown as peak I in curves III and IV. W_f is unbound water content in polymers whose transition temperature and enthalpy are equal to those of pure water (curve V):

$$W_c = W_{nf} + W_{fb} + W_f, \ (g/g) \quad (1)$$

From the cooling cycle data, the proportion of the amount of free water (W_f) is calculated by dividing the total area of the freezing water peak (Peak I) by the heat of crystallization of bulk water. The heat of crystallization is not constant for all water fractions, therefore, W_{fb} cannot be determined in the same way.

Ordinarily, the amount of W_{fb} is small compared with W_{nf} (g/g) and W_f (g/g). On this account, the total area of the $W_f + W_{fb}$ (g/g) (peaks I + II) per gram of dry sample is plotted as a function of W_c (g/g). The intercept of the linear plot is adopted as the amount of W_{nf} (g/g).

2.2. Bound water content determination by TG

Mass of water, mass of dry sample, temperature of dehydration and rate of dehydration can be evaluated by thermogravimetry. Modern TGs, working in a moderate temperature range, are designed for multi-purpose use. TGs are combined with various analyzers, such as differential thermal analyzer (DTA) (TG-DTA), Fourier transform infrared spectrometer (FT-IR) (TG-FTIR) and mass spectrometer (MS) (TG-MS). When TG-DTA is applied to water sorbing polymers, the heat of vaporization is simultaneously evaluated.

For the measurements, an aluminium open-type crucible (sample vessel) without a lid is ordinarily used, since the maximum temperature of measurements is at ca. 470 to 500 K. Gas flow rate markedly influences this type of measurement.

Mass loss starts immediately after water-sorbed sample is placed on the TG sample holder. Sample mass increases when the sample is dry compared with relative humidity at room temperature, or decreases if the sample sorbs a large amount of water compared with relative humidity. On this account, it is difficult to attain equilibrated conditions at around room temperature. The following techniques are commonly carried out:

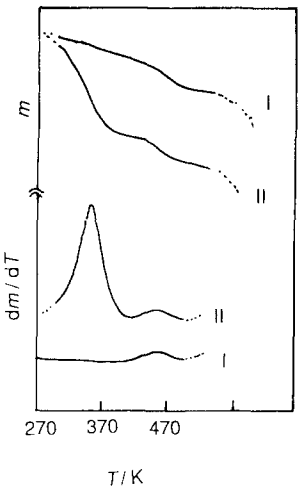

Fig. 2. Schematic TG curves and TG derivatograms of water sorbed on hydrophilic polymers: I – non-freezing water (W_{nf}); and II – $W_{nf} + W_f$.

1. the mass of starting temperature is extrapolated from the TG curve in steady state obtained at the high temperature side; and
2. the sample is frozen in a coolant, picked up from the coolant and placed on the TG sample holder, and scanned immediately.

When water molecules coexist with samples without any intermolecular interaction, mass loss (TG) and vaporization peak (DTA) terminates at a temperature lower than 373 K. In contrast, when water is tightly attached to polymers, mass loss is observed in two or multiple stages. Even if TG curves, apparently, show one stage, two or more peaks may be observed, if the derivatogram (dm/dT) is deconvoluted. DTA endotherms due to vaporization also show multiple peaks.

Fig. 2 shows schematic TG curves and TG derivatograms of polymer with non-freezing water (curve I, Fig. 2) and polymer with non-freezing water and free water (curve II). It is seen that the second state of vaporization is observed around 420 to 470 K. Peak temperature of the high-temperature side depends on the chemical structure of the sample. Non-freezing water evaporates at a temperature >373 K. The amount of each water fractions can be calculated from the area of each deconvoluted peak. The mass of water, calculated from the vaporization method, con-

tains several percent errors in the repeatability which mainly comes from sample setting in the TG sample holder. Results obtained by the TG method accord fairly well with those obtained by DSC [2].

2.3. Phase diagram of water-polymer systems

2.3.1. Glass-transition temperature (T_g)

Glass-transition temperature of various polymers in the presence of water is measured by DSC using a hermetically sealed sample vessel. T_g of hydrophilic polymers markedly decreases with the content of water; in some cases, a decrease of T_g was more than 150 K in the presence of 0.10 g/g water. It is necessary to choose a broad temperature range in order to cover T_g variation of polymers in the presence of water.

2.3.2. Melting, crystallization and liquid crystallization

DSC measurements of melting and crystallization of pure water are not always easy due to high surface tension of water. Contact surface between the sample vessel and water droplet is small. On this account, the peak of melting or crystallization is broad and, apparent multiple peaks are frequently observed. In contrast, melting and crystallization of water sorbed on polymers are easily measured by DSC. Transition temperature and enthalpy of sorbed water can be determined by the usual methods [3,4]. Temperature calibration is ordinarily carried out using melting and crystal–crystal transition temperature of cylohexane. Phase diagram can be established using peak temperature (T_p), or starting temperature of transitions (T_i). It is noteworthy that the bound water defined in Section 2.1 is in a thermodynamically non-equilibrium state. This suggests that transition temperature depends on measurement conditions and thermal history of the sample. Phase diagram established in water–polymer systems should be defined in terms of the data of experimental conditions.

2.3.3. Liquid crystallization

Transition enthalpy of liquid crystallization in water–polymer systems is small. Highly sensitive measurement is necessary. In some cases, transition of liquid crystallization cannot be observed, even if the liquid-crystal state is confirmed by morphological observation. Various reasons are suggested, such as low transition enthalpy value, broad transition temperature range, etc. In order to confirm the liquid-crystal transition, morphological observation is ordinarily carried out on the same sample.

2.3.4. Gel–sol transition

Transition enthalpy of gel–sol transition is small. Hence, a highly sensitive measurement is necessary.

2.4. Thermomechanometry

2.4.1. Thermomechanical analysis

Thermomechanical analyzers (TMA) controlled under humid conditions are commercially available. Manufacturers provide various types of attachment which are equipped with the standard TMA. A glass sample cell, in which the polymer sample is dipped in water is also available. The temperature range is limited due to the conformation of attachment.

2.4.2. Dynamic mechanical analysis

A dynamics mechanical analyzer (DMA) which can scan relative humidity in a controlled rate at a constant temperature was developed by users [5]. A DMA can be operated at a constant relative humidity was also designed by users. At present, DMA which can scan either temperature or relative humidity is commercially available.

2.5. Miscellaneous

2.5.1. Dielectric measurement

Dielectric measurement of polymers the presence of water is not suitable for the investigation of water–polymer interaction due to high dipole moment of water molecules. Dielectric measurements have been carried out in isothermal conditions, i.e. frequency was varied in a wide range at a constant temperature, and the temperature increased step by step. This method takes a long time to scan a sample in the entire temperature range of measurement. Conformation of sample cell and attachment of electroconductive paste or metal deposition to the sample surface are not suitable for water sorbing polymers. Due to the aforementioned facts, dielectric measurement has not been categorized as an appropriate method for the study of water sorbed polymers, although attempts were made to measure the aqueous solutions of hydro-

philic polymers at a subzero temperature [6]. Recently, Fourier transform dielectric measurements have been established [7]. By using this method, the temperature is scanned in a way similar to that of DSC. Application of this new method to water sorbed polymer was reported [8].

2.5.2. Alternative current calorimetry

AC calorimetry (ACC) [9] was developed by users. Among them, a glass sample holder capable of maintaining the water sorbed sample was reported [10]. Commercially available ACC mainly concerns the dry samples [1].

3. Interaction between water and water-insoluble polymers

Various natural and synthetic polymers, which have hydrophilic groups such as hydroxyl, carboxyl and carbonyl, have strong or weak interaction with water. Through this interaction, physical properties such as thermal properties of both, polymers and water are markedly influenced.

3.1. Interaction between water and cellulose

Cellulose is the most important hydrophilic, though water-insoluble, polysaccharide which consists of plant cell walls. Many authors have reported that water sorbed by cellulose has properties that are markedly different from free water [11–17]. Magne et al. [11,12] reported that melting and crystallization temperatures of the bound water in hydrophilic polymers such as cellulose and keratin are lower than those of free water. It has been considered that this difference in water properties is caused by the restriction of the molecular motion of water. Accordingly, in this section the properties of water, sorbed on cellulose, and the amount of water, bound to the hydroxyl groups of cellulose, will be discussed.

3.1.1. Typical DSC curves of water adsorbed on cellulose

Fig. 1 shows the schematic DSC curves of water sorbed on cellulose. When a cellulose sample containing water was cooled from room temperature to 150 K, the first-order transition was not observed until

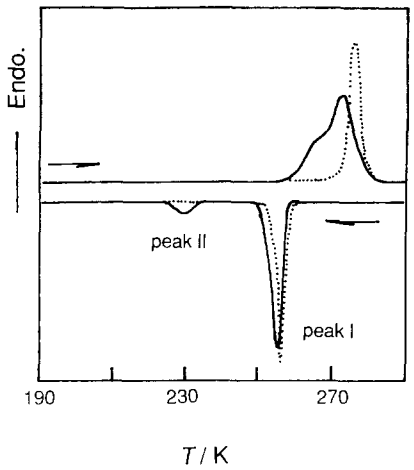

Fig. 3. Schematic DSC curves of water sorbed on various cellulose samples: (———) – adsorbed water; and (· · ·) – bulk water. Scanning rate=8 K/min; sample weight – ca. 5 mg; and $W_c = 0.8$ (g/g).

the water content exceeded a certain amount of water. After exceeding this water content, a broad crystallization peak (peak II) was observed in the ≈220–230 K range. When the amount of water, sorbed in cellulose, exceeded a certain value, at which the height of peak II reaches a maximum, a new sharp peak (peak I) appeared. The shape and the transition temperature of peak I accords well with that for the crystallization of pure water which is shown as the dotted line in Fig. 3.

In the DSC heating curve, as shown in Fig. 3., the endothermic peak of the water sorbed on cellulose appears at a temperature lower than that which corresponds to pure water. The shape of the endothermic peak varies according to the water content and also according to the kind of cellulose sample, such as cotton or jute. In some cases, a shoulder was found in the lower temperature side of an endothermic peak. In general, asymmetry was observed as a characteristic pattern of the melting of sorbed water on a hydrophilic polymer, such as cellulose.

3.1.2. Calculation of the amount of bound water with cellulose

In the case of crystallization of water sorbed on cellulose samples, the sum of the mass of water calculated from enthalpies of peaks I and II is less than the total amount added to the dry sample. As

mentioned previously, in the Section 2.1.2, the amount of water, corresponding to the difference between the added water and the amount of water calculated, is known as non-freezing water. The non-freezing water has none of the first-order transition and does not have any kind of crystalline structure. Freezing bound water content (W_{fb}) (corresponding to peak II in the DSC cooling curve) and free content (W_f) (corresponding to peak I in the DSC cooling curve) must have a certain kind of crystalline structure which may be the same as the structure of natural ice. There are nine polymorphic forms of ice possible, such as ice I, Ic, II, III, IV, V, VI, VII and VIII reported [16]. However, the structures from ice IV to ice VII are found only at very high pressures. Accordingly, in the usual experimental conditions that treat the above kinds of water sorbed on polymers, the possible structures of ice for freezing bound water can be considered to be ice I, Ic, II and III. The maximum value of melting enthalpy of ice (ice I) is estimated as 334 J/g, and the minimum value of melting of ice (ice III) is estimated as 311 J/g from the phase diagram of water [18]. It is considered that the estimated enthalpy error caused by the structure of ice seems to be <1%.

Therefore, as mentioned previously, Eq. (1) holds within the above-mentioned error range. Accordingly, the mass of bound water (W_b) is given as follows.

$$W_b = W_{nf} + W_{fb} \tag{2}$$

The percentage of bound water content, C_b, is calculated according to the following:

$$C_b = W_b/W_s \times 100(\%) \tag{3}$$

where W_s is weight of the sample.

Fig. 4 shows the relationship between the degree of crystallinity of cellulose samples and contents of bound water and non-freezing water [16]. Crystallinity of cellulose samples was measured by X-ray diffractometry. Amorphous cellulose was prepared by saponification of cellulose triacetate using sodium ethyl alcohol in dehydrated conditions. The amorphous cellulose was used as a standard material for the crystallinity calculation. Both, bound water and non-freezing water contents decrease with the increasing degree of crystallinity of cellulose samples. It is observed that the amount of freezing bound water (peak II) decreases with the increasing degree of

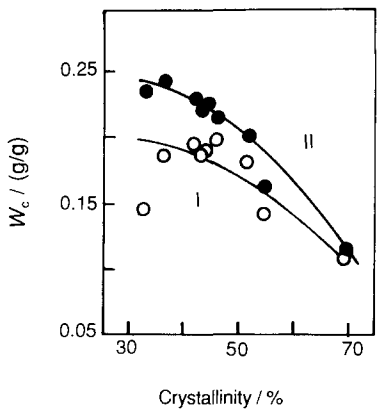

Fig. 4. The relationship between the degree of crystallinity of cellulose samples and contents of bound water (W_b) and non-freezing water (W_{nf}): I – W_{nf}; II – $W_b=W_{nf}+W_{fb}$ (see text).

crystallinity of cellulose samples. This fact suggests that only cellulose molecules in the amorphous region can be regarded as the adsorption site of water molecules.

The number of bound water molecules, M_b, sorbed on a glucose unit of cellulose can be calculated according to the following:

$$M_b \equiv (162 \times W_b)/(18 \times W_s) = (9 \times W_b)/W_s \equiv 0.09C_b \tag{4}$$

where the numerals 162 and 18 are molecular weights of glucose unit of cellulose and of water. The number of bound water molecules sorbed on a glucose unit in the amorphous region of cellulose samples, M_{ba}, is calculated according to the following:

$$M_{ba} = (M_b \times 100)/(100 - \text{degree of crystallinity}) \tag{5}$$

Fig. 5 shows the relationship between degree of crystallinity of cellulose and the number of bound water molecules (M_b) sorbed on a glucose unit of cellulose molecules and those (M_{ba}) in the amorphous region of cellulose [16]. As seen in Fig. 5, M_b decreases with increasing degree of crystallinity of cellulose in a way similar to that of bound water content, while M_{ba} is nearly constant at ca. 3.4 mol per glucose unit. This fact suggests that bound water attaches three hydroxyl groups in the amorphous region of cellulose.

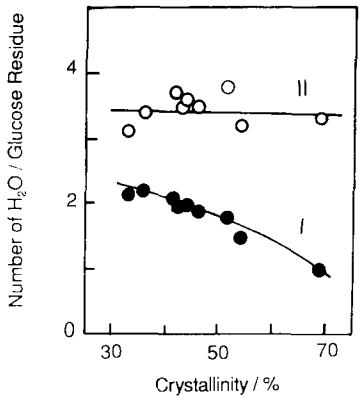

Fig. 5. The relationships between the degree of crystallinity of cellulose samples and the number of bound water molecules on a glucose unit of cellulose molecules (M_b) and those in the amorphous region of samples (M_{ba}): I – M_b; and II – M_{ba}.

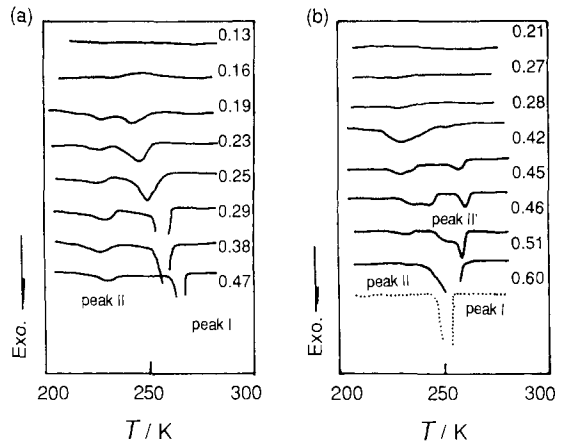

Fig. 6. Stacked DSC cooling curves of water sorbed on (a) – cellulose I and (b) – cellulose II: (———) – sorbed water; and (· · ·) – bulk water cooling rate=10 K/min. Numerals in the figures show water content (W_c) in (g/g).

3.2. *Structural change of the amorphous region of cellulose with the presence of water*

The higher order structure of cellulose has been explained by the two-state model for more than half a century. In this model, it has been considered that the amorphous region has a homogeneous structure. However, the result shown in our previous papers [19,20,21] indicated that the amorphous region of cellulose was difficult to consider as a homogeneous state, especially when the cellulose coexisted with water molecules. It was also suggested that the amorphous region of cellulose was reversibly transformed to the crystalline region when the non-freezing water became bound to the hydroxyl group [16,22,23]. Accordingly, in this section, the difference in water behaviour between celluloses I and II with the water content will be discussed. Cellulose I, which is separated from plant materials, has high molecular mass and shows high crystallinity. In contrast, cellulose II, which is regenerated from cellulose I via solving processes, has low molecular mass and the crystallinity is comparatively small.

3.2.1. *DSC curves of water sorbed on celluloses I and II*

Fig. 6(a and b) show the stacked DSC cooling curves of water sorbed on cellulose I and cellulose II, respectively [24]. The broken line in Fig. 6(b) corresponds to the crystallization curve of pure water. As shown in Fig. 6(a and b), no crystallization peak was observed when W_c of cellulose I is below 0.15 (g/g) and that of cellulose II below 0.25 (g/g). These facts suggest that, below the aforementioned W_cs, only non-freezing water exists in the above cellulose-I- and cellulose-II-water systems. When W_c exceeded critical amounts for celluloses I and II, peak II was first observed. It is considered that peak II represents the irregular structure of ice formed under the influence of the hydroxyl group of cellulose molecules.

The crystallization behaviour of water in cellulose II is complicated. When W_c is between 0.3 and 0.6 (g/g), an intermediate peak (peak II′) appears at a temperature higher than that for peak II, but lower than that for peak I, as shown in Fig. 6(b). Peak II′ shifts to the higher temperature side with increasing W_c, becoming a shoulder of peak I when W_c is >0.5. Accordingly, it is considered that peak II′ also corresponds to the bound water [25].

When W_c exceeds a certain value (0.19 (g/g) for cellulose I and 0.42 (g/g) for cellulose II), peak I appears. However, when W_c is low, peak I appears at a temperature lower than that of the normal crystallization temperature of free water which is higher than that of bulk water. This suggests that peak I is also under the influence of cellulose matrix.

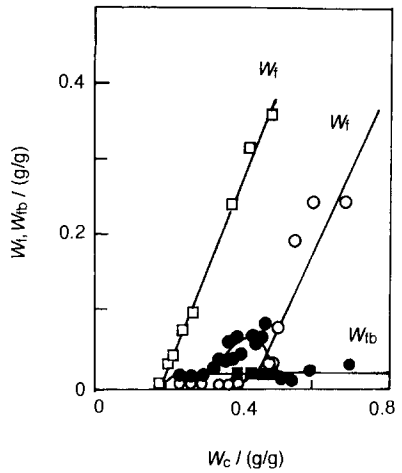

Fig. 7. The relationship between amount of freezing water (W_f), freezing bound water (W_{fb}) and water content (W_c) sorbed on (□, ■) cellulose I and (○, ●) cellulose II. (□,○) – W_f, and (■, ●) – W_{fb}.

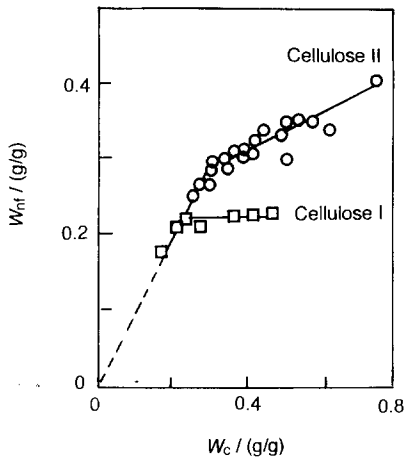

Fig. 8. The relationships between amount of non-freezing water (W_{nf}) and water content (W_c) sorbed on (□) cellulose I and (○) cellulose II.

3.2.2. *Structural change of cellulose I and II with water*

Fig. 7 shows variation of W_f and W_{fb} of cellulose I and II, respectively, as a function of W_c [24]. W_f of cellulose I first appeared at around W_c=0.16 (g/g) and then increased with increasing W_c. In the case of cellulose II, W_f first appeared at ca. W_c = 0.40 (g/g) and increased with increasing W_c. This fact indicates that the amorphous region of cellulose II is larger than that of cellulose I. It was also observed that the behaviour of W_{fb} of cellulose II is different from that of cellulose I. W_{fb} of cellulose I appears at ca. W_c=0.16 (g/g) and levels off quickly when W_c exceeds 0.2, as shown in Fig. 7. W_{fb} of cellulose II (peak I and peak II) increases from W_c at ca. 0.25 (g/g) and reaches a maximum value at ca. W_c=0.40 (g/g), then decreases and levels off when W_c exceeds 0.50 (g/g). This maximum value coincides with the W_c where W_f appears, as shown in Fig. 7. The foregoing facts suggest that the size and regularity of ice, that is considered to be influenced by the structural change of the cellulose matrix, change with W_c. This means that the molecular arrangement of cellulose II changed distinguishably by the diffusion of water molecules into the amorphous region with increasing W_c. When the crystal size of ice with cellulose II exceeded a critical point, which corresponded to W_c=0.50 (g/g), the ice merged into ordinary ice and, accordingly W_{fb} decreased. On the other hand, it is considered that the molecular arrangement of cellulose I initially caused a transformation into a more ordered state, so that a decrease of heat capacity of the water–cellulose I system was observed [26]. After that, the structure of cellulose scarcely changed with increasing W_c and, accordingly, W_{fb} of cellulose I was almost the same throughout the W_c over a certain value.

Fig. 8 shows the relationship between W_{nf} and W_c of celluloses I and II. The W_{nf} value for cellulose I is almost constant when W_c is over ca. 0.2 (g/g), while that for cellulose II gradually increases with increasing W_c. The foregoing facts suggest that the amorphous region of cellulose I takes a more ordered structure with a small amount of water and this structure is stable, even with the sorption of more water. However, the amorphous region of cellulose II is not stabilized by forming an ordered structure, but increases gradually with the further sorption of more water. These results were also supported by the X-ray diffraction data. The X-ray diffractograms of cellulose I showed that the peak reflecting (002) plane became more pronounced with increasing W_c, showing the increase of the ordered structure with the sorption of water. On the other hand, the peak reflecting (022) plane of cellulose II decreased and became flatter with increasing W_c, showing the crystallinity of cellulose II [27]. It was observed that the breaking strength of cellulose I increased with sorption of a small amount of water [27].

3.3. Interaction between water and lignin

Lignin is the second major component of wood. The chemical structure of lignin is known to have several chemical groups, such as 4-hydroxyl, guaiacyl and syringyl groups. As the phenyl groups constitute the basic chain unit of lignin molecules, it may be categorized as a hydrophobic polymer. However, a certain portion of the hydroxyl groups of lignin molecules facilitate a limited interaction with water. In living wood, cellulose–lignin–water comprises a complicated composite material. Accordingly, in this section, it was attempted to quantitatively estimate the structural change of water with lignin matrix, using methylated DL (MDL) and acetylated DL (ADL) 1,4-dioxane lignin (DL) as samples. The change of the glass-transition temperature of lignin affected by sorbed water was also estimated.

3.3.1. Bound water associated with lignin

Fig. 9 shows the change of W_f, W_{fb} and W_{nf} with W_c. The critical value of W_{nf} is found to be W_c=ca. 0.08–0.09 (g/g), corresponding to the point where W_{fb} emerges. The W_{nf} value slowly increases over this W_c. This suggests that the structure of DL molecules changes slightly with increasing W_c, showing that the diffusion of water molecules into DL matrix takes place [28].

3.3.2. Influence of sorbed water on hydrogen bonding of lignin

Fig. 10 shows a three-dimensional relationship between T_g of DL, W_c and degree of acetylation of DL. In this figure, point E represents the T_g of DL and point F the T_g of ADL which has 100% relative degree of acetylation of DL. Line AB shows the levelling off of T_g. The T_g of dry DL decreases markedly when water is added. T_g of variously acetylated DLs decreases with increasing W_c. T_g of DL decreased with acetylation in the similar manner. The plane EFGH is divided by the plane ABIJ. The ABEF section of the plane shows the decrease in T_g of variously acetylated DL with W_c. The ABGH section of the plane is almost flat and represents the region in which no further breakage of hydrogen bonding occurs. T_gs of both, acetylated and non-acetylated DLs decrease sharply in the region up to Wc=0.1 (g/g). Accordingly, it can be assumed that water molecules act as a hydrogen-bond breaker below $W_c = 0.1$ (g/g) in the lignin–water systems. It is clear that the hydroxyl groups of lignin play an important role in the formation of hydrogen bonds in lignin. It is also seen that the excess free water in lignin does not distinguishably affect the T_g of lignin.

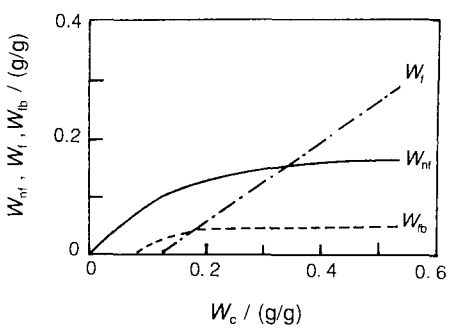

Fig. 9. The relationship between amount of freezing water (W_f), freezing bound water (W_{fb}), non-freezing water and water content (W_c) sorbed on lignin.

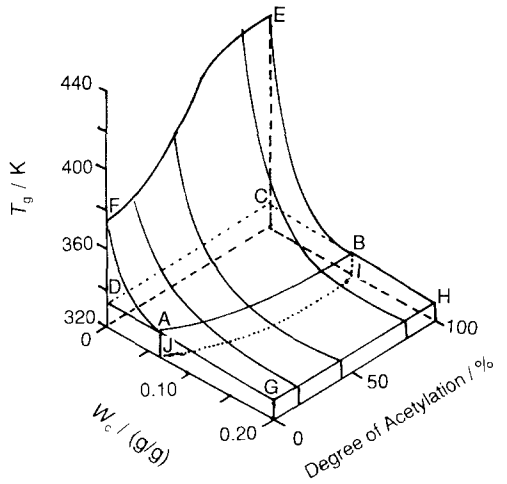

Fig. 10. Three-dimensional diagram between glass transition (T_g),. water content (W_c) and degree of acetylation of 1,4-dioxane lignin (DL).

3.4. Interaction between water and polyhydroxystyrene derivatives

The chemical structure of polystyrene derivatives such as poly(4-hydroxystyrene) (PHS) and poly(4-hydroxy-3-methoxystyrene) (PHMS) are related to

the 4-hydroxyphenyl and guaiacyl groups in lignin. These polystyrene derivatives have some advantageous mechanical properties such as high breaking strength compared with that of usual polystyrene [29].

The glass-transition temperatures (T_gs) of these polystyrene derivatives are ca. 20–80°C higher than those of polystyrenes [30]. The above facts have been attributed to the hydrogen bonds which formed between hydroxyl groups of the polyhydroxystyrene derivatives. Accordingly, in this section, the effect of water on the hydrogen bonding of polyhydroxystyrene derivatives will be discussed.

3.4.1. *Change of glass-transition temperatures of polyhydroxystyrene derivatives with water*

Figs. 11 and 12 show three-dimensional diagrams for partially hydrolyzed poly(4-acetoxystyrene) (PAS) and poly(4-acetoxy-3-methoxystyrene) (PAMS) with T_g on the vertical axis, and W_c and degree of hydrolysis of PAS and PAMS on the horizontal axes. In Figs. 11 and 12, the point E shows the T_gs of PHS and PHMS (PHS=455 K and PHMS=415 K), the other point, F, shows T_gs of PAS and PAMS (PAS=385 K and PAMS=388 K) and the point D shows the T_g of polystyrene (PSt=365 K) which was used as a reference material. The plane ABCD shows the isothermal plane of the T_g of PSt. The T_gs of PHS and PHMS decrease rapidly with water sorption, suggesting the breakage of intermolecular hydrogen bonding by the effect of water molecules. The plane EFGH is separated by the plane ABIJ. The separated plane ABEF has a steep gradient, while the plane ABHG has a gradual gradient. The planes ABEF in Figs. 11 and 12 show the decrease of T_gs of partially hydrolyzed PAS and PAMS by the breakage of hydrogen bonding with the sorption of water. The planes ABHG in both figures are considered to show the decrease of T_g by the plasticizing effect of water with partially hydrolyzed PAS and PAMS samples. The excess water molecules in partially hydrolyzed PAS and PAMS remain as the bulk water in the W_c range over certain amounts which are shown as the planes ABIJ in Figs. 11 and 12. This excess water has plasticizing effect on the polymers.

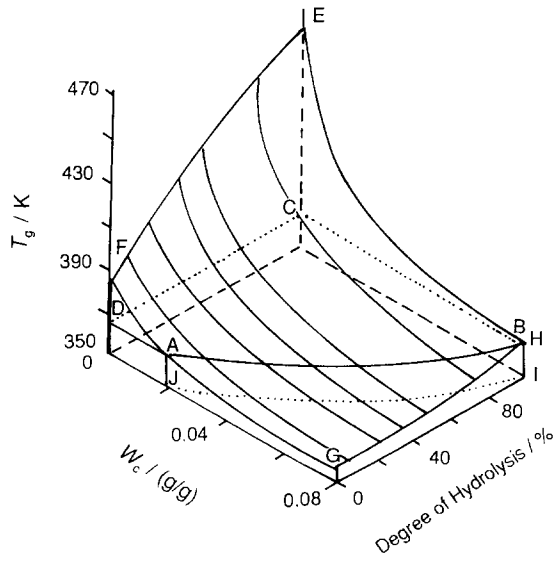

Fig. 11. Three-dimensional diagram between glass transition (T_g), water content (W_c) and degree of hydrolysis of poly(4-acetoxy styrene) (PAS).

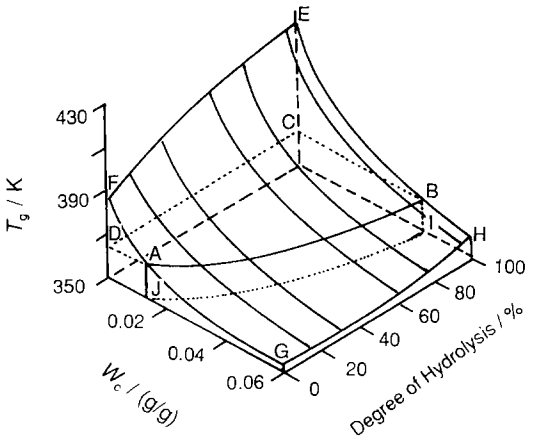

Fig. 12. Three-dimensional diagram between glass transition (T_g), water content (W_c) and degree of hydrolysis of poly(4-acetoxy, 3-methoxystyrene) (PAMS).

From the foregoing result, it can be concluded that the hydroxyl groups of the substituents in hydrolyzed PAS and PAMS have an important role in the formation of intermolecular hydrogen bonding. The difference between the T_gs of PAS and PAMS and their partially hydrolyzed derivatives may be due to the effect of the methoxyl groups introduced into the 3-position of the aromatic ring. Water sorbed on the partially hydrolyzed PAS and PAMS derivatives acts as a hydrogen-bond breaker, in case W_c is less than a

certain amount, and acts as a plasticizer above this value of W_c.

3.5. Interaction between water and poly(ethylene terephthalate)

Most synthetic polymers are ordinarily hydrophobic, and it has been thought that physical properties of the polymers are not affected by the presence of water. Recently, however, the water in synthetic polymers such as poly(ethylene terephthalate) (PET) has received attention since, even a small amount of water captured by synthetic polymers is known to decrease the reliability such as dimension stability and durability, when these polymers are used in industrial applications such as recording materials and electrical devices. Accordingly, in this section, attention will be focussed on the phase transition of PET in the presence of water.

3.5.1. Effect of water on the molecular motion of PET

Fig. 13 shows the DSC curves of PET with various water contents. T_g is observed as the baseline deviation and, at temperatures between 333 and 335 K, sub-T_gs are observed when W_c exceeds 0.029 (g/g) [31]. For the observation of the above phase transition of PET in water, the PET sample was firstly heated up to 380 K in order to accelerate the diffusion of water into the polymer matrix. It is known that the enthalpy relaxation occurs when a PET sample is kept for a long time at room temperature [32]. Water is also known to increase the rate of enthalpy relaxation [33].

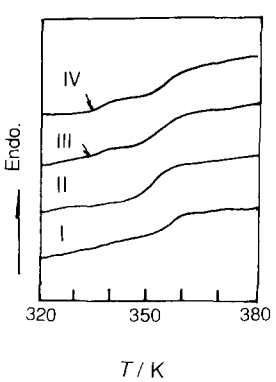

Fig. 13. DSC heating curves of poly(ethylene terephtalate) containing various amounts of water at around glass-transition temperature (T_g). I – 0; II – 0.007 (g/g); III – 0.029 (g/g); and IV – 0.061 (g/g). Arrow shows sub-T_g.

Temperature and time are counteracting factors in treating the change of phase transition and also the structural change of PET. When PET samples are treated, therefore, the errors unavoidably deriving from the thermal history of each PET sample must be taken into account. Thermal and viscoelastic data of sub-T_g of PET and its molecular implications have been reported by some authors [34–36]. The molecular mechanism of the above phenomena has not yet been sufficiently explained at present. However, it can be at least said from the data shown in Fig. 13 that the excess water with PET accelerates nucleation and molecular transportation of PET in the glassy state.

4. Water soluble polymers

Polymers having hydrophilic groups such as hydroxyl, carboxyl and sulfonate groups tend to solve in water. Polysaccharides are usually water soluble. Various kinds of polysaccharide molecules accept a random structure in a dilute aqueous solution at a temperature higher than the critical temperature, e.g. get–sol transition temperature. When the solution is cooled, random molecular chains ordinarily form helical structures, and the helical chains congregate into hydrogel or liquid-crystal form, depending on the concentration, thermal treatment, and the presence of various kinds of ion. In this section, representative polysaccharides forming hydrogels and/or liquid crystals are introduced. At the same time, gelling properties of poly(vinyl alcohol) are described as an example of synthetic water soluble polymer.

4.1. Hydrogels

4.1.1. Hyaluronic acid

The molecular configuration and structure of the repeating disaccharide unit of hyaluronic acid is shown in Fig. 14. The long linear chain is unbalanced, and at physiological pH, due to its polyanionic character, exhibits considerable stiffness, which is responsible for its large hydrated volume. Light scattering shows that the long branched chain can form a random coil occupying molecular domain containing a large

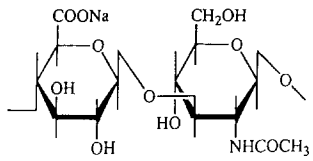

Fig. 14. Chemical structure of hyaluronic acid.

amount of water. The hyaluronic acid needs to have a molecular weight in excess of 2×10^6 to form such a large hydrated volume with a diameter of ≈300 nm. Hydrodynamic measurement indicates that radius of gyration is almost the same as the radius of the solved sphere (Random-Coil-Solvated Sphere Model). Hyaluronic acid has a considerably greater ability to trap water than other polyelectrolyte polysaccharides. A 2% solution of pure hyaluronic acid holds the water so tightly that it looks like a gel showing elastic or pseudoelastic properties. The combination of high molecular weight, and large molecular volume forces the overlap between individual hyaluronic and molecular domains, resulting in extensive chain entanglement and chain–chain interaction [37–40].

Hyaluronic acid is widely applied in the medical field [41,42] due to its high compatibility with animal tissue. Due to its high water-retaining ability, hyaluronic acid is added to cosmetics. It is also reported that hyaluronic acid is blended with various hydrophilic polymers for the purpose of increasing the swelling properties of water.

Phase transition behaviour of water of hyaluronic acid is investigated by DSC in a wide range of water contents (Fig. 15). The samples were heated at 10 K/min after cooling from 330 to 150 K at a cooling rate of 10 K/min [43–45]. The sample with W_c=0.5 (g/g) did not show any phase transition except for a shift in the baseline due to glass transition (T_g). The heat capacity difference at T_g of water–hyaluronic acid system is particularly large among various water–polyelectrolyte polysaccharide systems. A characteristic feature of the glassy state of hyaluronic acid is explained by a large amount of amorphous ice which is formed during the quenching process in the network structure [46,47]. Fig. 16 shows a phase diagram of water–hyaluronic acid systems. T_g decreases markedly until W_c=1.0, (g/g), and reaches a minimum at around W_c=1.1. (g/g).

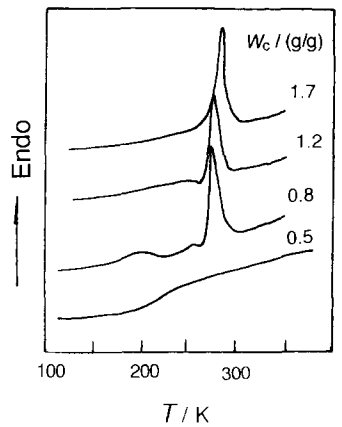

Fig. 15. DSC heating curves of water–hyaluronic acid systems with various water contents (W_c). Heating rate=10 K/min.

The melting curves of hyaluronic acid–water systems show the multiple peaks having a shoulder at the low temperature side of the main peak. Fig. 17 shows the relationship between starting temperature (T'_{im}), T_{pmII}, the melting peak (T_{pmI}) and temperature of crystallization (T_c). T'_{pi} and T_{pmII} linearly increase with increasing T_c. In contrast, T_{pmI}s are maintained at a constant value. This indicates that melting of irregular ice formed in the hyaluronic acid network is observed at the lower temperature side peak [47]. Isothermal crystallization of hyaluronic acid having various W_cs was carried out at different temperatures

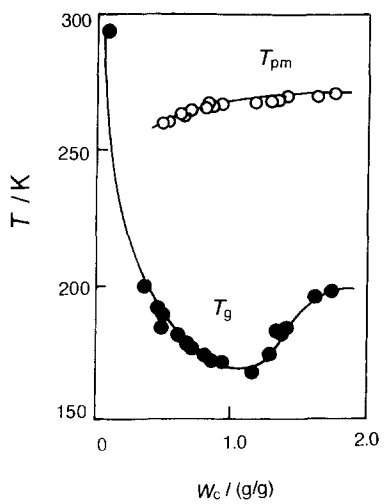

Fig. 16. Phase diagram of the water–hyaluronic acid system.

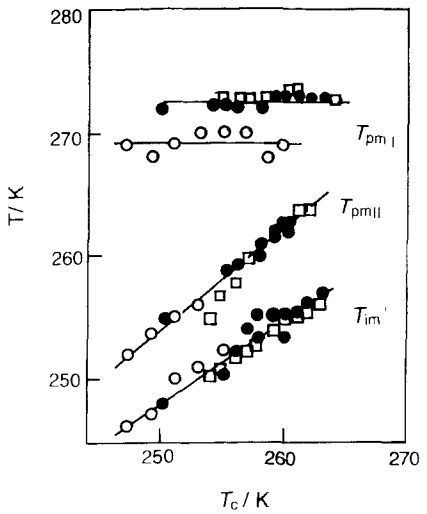

Fig. 17. The relationships between peak temperature of melting (T_{pmI}), peak temperature of sub-melting (T_{pmII}), starting temperature of melting (T'_{im}) and crystallization temperature (T_c) of water–hyaluronic acid systems: (○) – W_c=1.2 (g/g); (●) – 1.5 (g/g); and (□) – 2.1 (g/g).

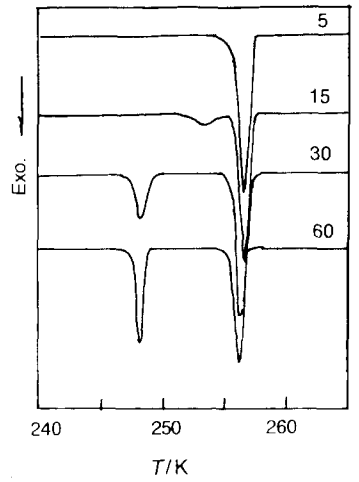

Fig. 19. DSC cooling curves of gallan gel (concentration=1.2 mg/10 ml of water) held at 365 K for various times. Numerals in the figure show holding time in min. Cooling rate – 10 K/min.

[48]. It was found that the rate of nucleation of water in hyaluronic acid gel was almost the same as bulk water. In contrast, the rate of crystal growth of freezing bound water was ca. 10 times slower than that of bulk water.

4.1.2. Gellan gum

Gellan gum is the extracellular, anionic polysaccharide produced by the bacterium *Pseudomonas elodea*. The chemical structure of gellan gum is shown in Fig. 18. Aqueous gellan solutions, above a threshold concentration level, form gels. Gellan gels are utilized in food industry, on account of its flexibility and transparency [49]. The characteristics of these gels depend not only on the gellan concentration but also on the valency and size of cations present in the solutions. It is noteworthy that water played a crucial

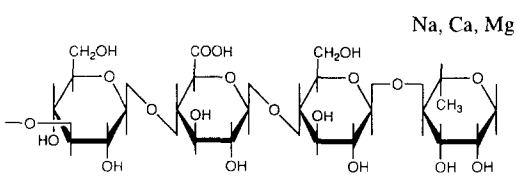

Fig. 18. Chemical structure of gallan gum.

role in the formation of crystalline regions in gellan [50,51]. In order to stabilize the double helix, cations and the carboxylic groups are coordinated. At the same time, it has been suggested that polyion–cation–water–cation–polyion bridges may bind the double helices together to form a junction zone [51,52]

Aqueous gellan solution of concentration 1.2 mg of gellan gum/10 ml of water was hermetically sealed, placed in an oven and pre-heated to 313 K for 24 h [53]. The gellan gum used was an 'ordinary sample' obtained from the research group on gellan gum affiliated to the Society of Polymer Science, Japan [53–56]. These samples were heated in a DSC at 10 K/min from 293 to 365 K, and held for 5 min before being cooled at the same rate to 130 K. The same sample was reheated to 365 K, held at that temperature for various holding times and recycled. Fig. 19 shows DSC cooling curves of the sample held for various times at 365 K. The single exotherm which is initially observed on cooling is replaced by a structural peak and ultimately by two peaks as the holding time is increased. A similar series of observations was made on samples with various concentrations at holding temperatures of 350 and 340 K. A change of relative size of the exotherms indicated that the progressive shift in relative areas of the peak proceeds more slowly at lower holding temperatures.

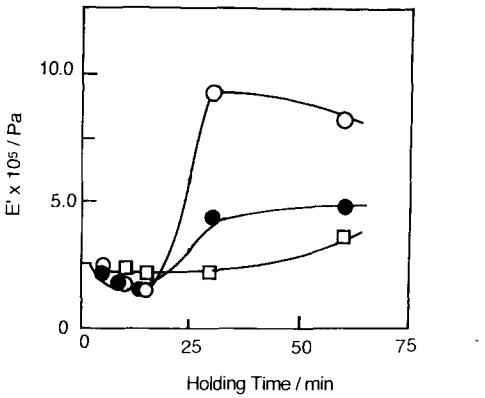

Fig. 20. The variation in elastic modulus (E') with holding time at various temperatures of gallan gel (concentration=1.2 mg/10 ml of water): (○) – 365; (●) – 350; and (□) – 340 K.

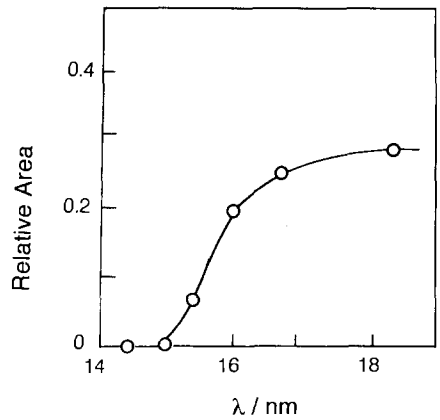

Fig. 21. The relationship between relative area of exotherms and size of junction zone (λ) of gallan gel (concentration=1.2 mg/10 ml of water).

Elastic modulus (E') of the above-mentioned sample was measured using a thermomechanical analyzer. Increase in E' is observed after ca. 25 min holding for all samples held at 340, 350 and 360 K, as shown in Fig. 20 [53]. Small-angle X-ray scattering (SAXS) was carried out using synchrotron orbital radiation (SOR). Thermal and X-ray results suggested that the individual double helices are bound by cationic interactions and inter-molecular hydrogen bonding. The junction zones are linked in the form of extended helical chain. The concentration of ordered regions increases on annealing, as can be observed by the increase in the low-temperature exotherm, suggesting the increase of bound water.

Fig. 21 shows the relationship between relative area of exotherms [(area of the low-temperature exotherm)/(area of the high-temperature exotherm)] shown in Fig. 19 and size of the junction zone estimated by SAXS. It is clearly seen that the amount of bound water reflects the increase of the junction zone of gellan hydrogels [55].

Gel–sol transition behaviour is investigated using a highly sensitive DSC from with respect of gelling ability of gellan in the presence of various types of cations [56].

4.1.3. Xanthan gum

Xanthan gum is an anionic extracellular polysaccharide produced by the bacterium *Zanthomonas campestris*. The chemical structure of xanthan is shown in Fig. 22. The chemical and physical properties of xanthan and its commercial applications are described in detail elsewhere [57]. In the solid state, xanthan adopts a double helical conformation in the presence of a nominal amount of water [58]. Dilute solution >0.5% forms gels. The junction zones are thought to be linked by extended helical chains, resulting in a three-dimensional network [53,59]. Various liquid-crystal forms of xanthan have been reported over a wide range of water contents [60,61]. Xanthan gels exhibit a gel–sol transition in the region of 320 K, depending on concentration, molecular weight and on the nature of the cations present. The nature of the xanthan chains in the solution has been widely discussed [62,63].

Sample preparation for thermal measurements were the same as that of gellan hydrogels described in Section 4.1.2. An increase of freezing bound water is observed by DSC, as shown in Fig. 23, in the similar manner as shown previously (Fig. 19). The thermal

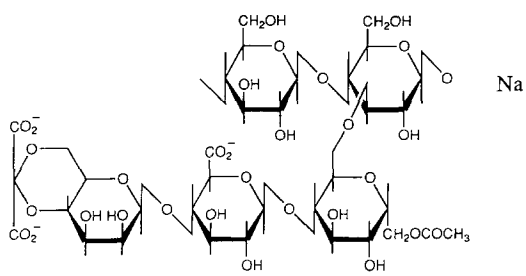

Fig. 22. Chemical structure of xanthan gum.

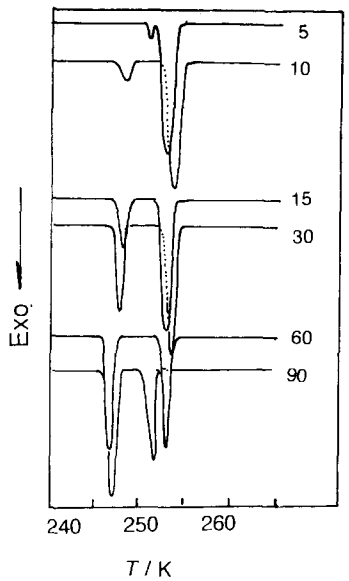

Fig. 23. DSC cooling curves of xanthan gel (concentration=2.0 mg/10 ml of water) held at 365 K. Numerals in the figure show holding time in minutes.

non-equilibrium nature of both sol and gel states of xanthan gels was confirmed [64].

4.1.4. Other polysaccharides

Besides the polysaccharides already mentined, the thermal properties of agarose [65,66], carrageenan [67,68], gum Arabic and its mixture [69], carboxymethylcellulose [70] and alginic acid [70,71] hydrogels have been investigated.

4.1.5. Poly(vinyl alcohol) (PVA)

PVA is known as a representative gel-forming synthetic polymer. When an aqueous solution of PVA is irradiated by ^{60}Co γ-ray, elastic and transparent gels are obtained. Cross-linking density can be evaluated by Flory's equations, using the data obtained by either swelling or mechanical method [72]. Fig. 24 shows DSC melting curves of water restrained in PVA gels as a function of cross-linking density ($1/M_c$) [73]. The melting pattern of ice in each gel is complicated; two main peaks with several small shoulder peaks are observed. These small shoulder peaks were affected by the repeated heating and cooling during DSC runs. W_f rapidly decreased with increasing cross-linking density. When $1/M_c$ increased above 2×10^{-4}, the amount of free water disappeared.

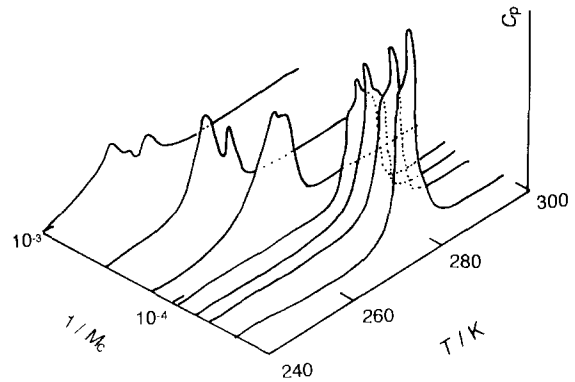

Fig. 24. DSC heating curves of water restrained in poly(vinyl alcohol) hydrogel with various cross-linking densities. Heating rate=10 K/min.

The amount of W_{nf} is almost constant, regardless of $1/M_c$, and W_{fb} decreased gradually with increasing $1/M_c$.

An aqueous solution of PVA is brought to gelation by freezing and defreezing [74,75,76]. The molecular chains are not chemically cross-linked, but exhibit a certain association resulting in the formation of a pseudo-gel. As shown in Fig. 25, a large amount of freezing bound water was confirmed in a pseudo-gel by DSC investigation [77].

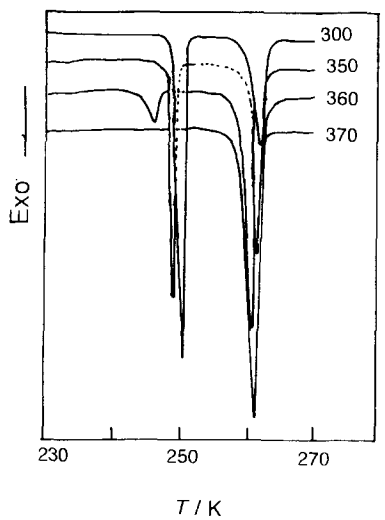

Fig. 25. DSC cooling curves of poly(vinyl alcohol) pseudo-gel held at various temperatures. Numerals in the figure shows holding temperature. Cooling rate=10 K/min.

4.2. *Formation of liquid-crystal structure in the water–polyelectrolyte system*

The possibility that an ordered structure is present in dilute solutions of ionic polymers has been reported by several authors [78,79–83], but attention has not been paid to the molecular arrangements of polyelectrolytes in highly concentrated aqueous solutions. Over the past few years, using DSC, nuclear magnetic resonance spectroscopy (NMR) and polarizing microscopy, the molecular behaviour of water–polyelectrolyte systems has been studied [43,46,48,54,61,84–100].

The experimental results reveal that polyelectrolytes in highly concentrated aqueous solutions have a unique property that is capable of forming a liquid-crystal phase. This characteristic originates from the fact that water molecules associated with polyelectrolytes have a conformation different from ordinary molecular packing. When water molecules are directly bonded to the ionic groups of polyelectrolytes, the mobility of the water decreases markedly [84,86,89,91,93–95,98].

DSC studies have shown that water molecules, directly associated with the ionic group, do not display a first-order phase transition [84,85,87–90,92–100]. NMR relaxation studies have also suggested that the molecular motion of water molecules around the ionic groups is markedly restricted, compared with that of free water [84,86,89,91,93–95,98]. However, the molecular behaviour of the water–polyelectrolyte system has not yet been fully understood. Accordingly, the recent advances in our studies on this system are given in the following section.

4.2.1. *Carboxymethylcellulose (CMC)*

Fig. 26 shows representative DSC curves of the water–sodium carboxymethylcellulose (NaCMC) system with W_c=1.26 (g/g). When the sample was cooled at a rate of 10 K/min, two exotherms were found at 268 and 245 K (curve I).

When the sample was reheated at 10 K/min (curve II), a step-wise change in the baseline at 190 K, a broad exotherm at ca. 240 K and two endothermic peaks at 265 and 330 K were observed. The large endothermic peak observed at 265 K was attributed to the melting of free water (T_m), as reported previously [88]. The small endothermic peak observed at 330 K

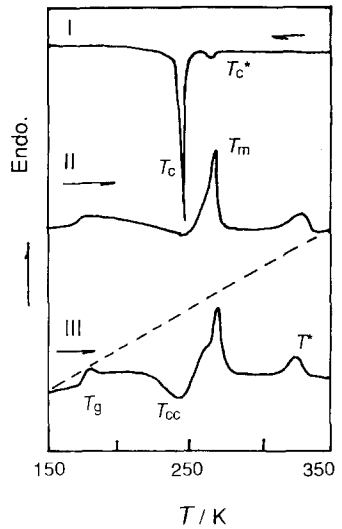

Fig. 26. DSC curves of water–carboxymethylcellulose systems. Heating and cooling rate=10 K/min.

was attributed to the transition (T^*) from the liquid-crystal state to the isotropic liquid state. This was supported by observations on the presence of the liquid-crystal phase in the temperature range between T_m and T^*, using a polarizing microscope. The peak corresponding to T^* appeared when W_c was ca. 0.4 (g/g). The peak temperature (T^*) decreased with increasing W_c and was barely observable when W_c was 1.5(g/g). When the sample was quenched from 320 to 150 K (curve III), the step-wise change in the baseline at 190 K and the exotherm at ca. 240 K became prominent. The temperature corresponding to the step-wise change in the baseline showed a heating-rate dependence. This change also showed enthalpy relaxation by slow cooling or annealing at a temperature, slightly lower than the endothermic deviation of the baseline. This transition was, therefore, attributed to glass transition (T_g). The exotherm at ca. 240 K was attributed to a cold crystallization (T_{cc}) of the system via which the glassy state was transformed to the crystalline state. Other water–CMC–metal-salt systems including LiCMC, KCMC and MgCMC showed similar phase transitions, as in Fig. 26, but the water–CMC systems with the divalent cations such as the water–MgCMC system required more time for the molecular rearrangement than systems with monovalent cations.

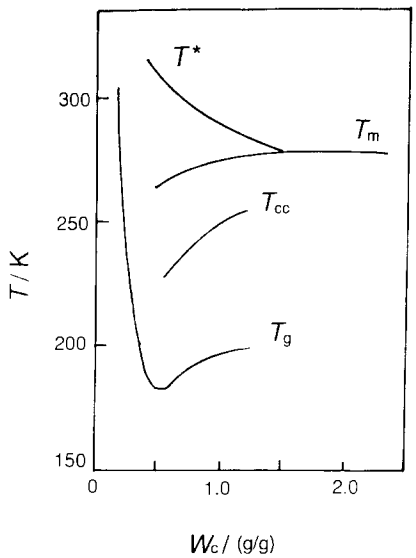

Fig. 27. Phase diagram of the quenched water–sodium cellulose sulfate systems: T_g – glass transition temperature; T_{cc} – cold-crystallization temperature; T_m – melting temperature; and T^* – liquid-crystal–liquid transition temperature.

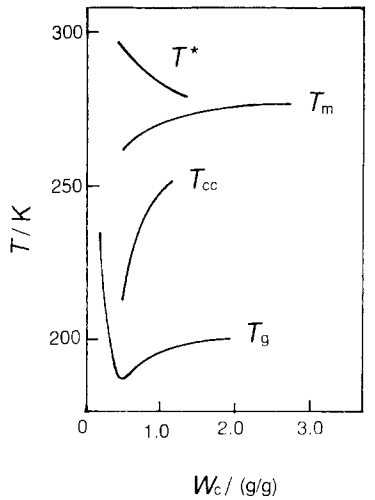

Fig. 28. Phase diagram of the quenched water–xanthan gum systems: T_g – glass-transition temperature; T_{cc} – cold-crystallization temperature; T_m – melting temperature; and T^* – liquid-crystal–liquid-transition temperature.

4.2.2. *SOdium cellulose sulphate (NaCS)*

Fig. 27 shows the phase diagram of the quenched water–NaCS system obtained from the similar DSC measurements as mentioned in the Section 4.2.1. This figure shows that the quenched system consists of glassy, crystalline, liquid-crystal and isotropic states. The transition temperature (T^*) from the liquid crystal to the isotropic liquid phase decreases with increasing W_c in the W_c range between ca. 0.4 and 1.4 (g/g), although melting and cold-crystallization temperatures (T_m and T_{cc}) increase with increasing W_c. However, T_g shows a minimum at ca. W_c=0.4 (g/g). This phenomenon is explained as follows: below W_c=0.4 (g/g), T_g of the system decreases with increasing W_c, because the molecular motion of the system increases with increasing W_{nf}, while above W_c=0.4 (g/g), T_g of the system increases because the formation of ice begins to restrict the molecular motion of the system with increasing W_f. The fact that both, the heat of the transition (ΔH) from the liquid-crystal phase to the isotropic liquid phase and the transition temperature (T^*) decrease with increasing W_c may suggest that the presence of mobile water molecules disturbs the regular alignment of NaCS molecules in the water–NaCS system.

The value of W_{nf} in the water–NaCS system was calculated as W_{nf}=0.38 (g/g). As shown in Fig. 27, the molecular rearrangement in the system starts when the value of W_c is more than ca. 0.4 (g/g). In this W_c range, NaCS molecules become mobile and form a regular alignment, showing a mesophase when W_c is <1.4 (g/g). If W_c exceeds this value, free water molecules start to disturb the regular alignment of the system.

4.2.3. *Xanthan gum*

Fig. 28 shows the phase diagram obtained from the DSC heating curves of the quenched water–xanthan systems with various W_cs. The value of T^* decreases with increasing W_c as was observed in the phase diagram for the water–NaCMC, the water–NaCMC and the water–NaCS systems. The W_c dependence of T^* suggests that the formation of the liquid-crystal phase depends strongly on W_c. The T_m value depends on W_c in the W_c range below 1.4 (g/g). The T_m of the samples, with W_c between 0.5 and 1.4 (g/g), is lower than that of pure water. In the same W_c range, the value of cold crystallization (T_{cc}) also depends on W_c. These facts suggest that water molecules in the water–xanthan system with W_c between 0.5 and 1.4 (g/g) are strongly affected by xanthan molecules. The water molecules are considered to be a kind of bound water. As shown in Fig. 28, the glass transition is observed in

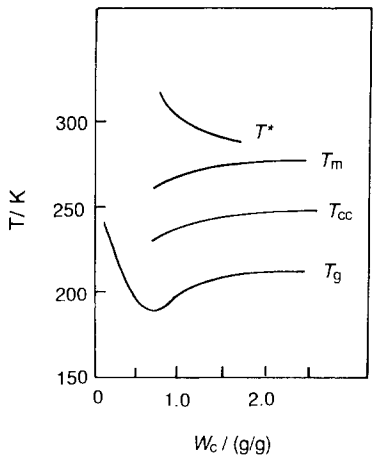

Fig. 29. Phase diagram of the quenched water–polystyrene sulfonate systems: T_g – transition temperature; T_{cc} – cold-crystallization temperature; T_m – melting temperature; and T^* – liquid-crystal–liquid transition temperature.

the water–xanthan system at a temperature below 200 K in W_c ranging from 0.5 to 2.0 (g/g), and the T_g value increases with increasing W_c in the W_c range above 0.5. However, in the W_c range below 0.5 (g/g), the T_g value decreases with increasing W_c with a minimum of T_g at W_c=ca. 0.5 (g/g). The reason of the appearance of this T_g minimum was previously explained.

4.2.4. Sodium polystyrene sulphonate (NaPS)

The water–NaPS system also showed the formation of the ordered structure which was observed in other polyeletrolytes, such as CMC, NaCS and xanthan.

Fig. 29 shows the phase diagram obtained from the DSC heating curves of the quenched water–NaPS (M_w=7.0 × 10^4) system with various W_cs. The value of T^* decreases with increasing W_c, as observed in the phase diagrams for the other water–polyelectrolyte systems. The melting peak of water was not observed in the W_c range less than ca. 0.6 (g/g). The value of T_m increases with increasing W_c, levelling off above W_c=ca. 1.3(g/g). The T_{cc} value shows the same tendency as the T_m in the W_c ranging between 0.6 and 1.3 (g/g). The glass transition also reveals a W_c dependence. The T_g value increases with W_c, when W_c is >0.6 (g/g). In the W_c range of <0.6 (g/g), the T_g value decreases with increasing W_c, and a T_g minimum is observed at W_c=ca. 0.6 (g/g).

The W_{nf} value in the water–NaPS system was calculated to be W_{nf}=0.62 (g/g) using the equations mentioned previously in Section 2. This value agrees well with the values shown in Fig. 29, suggesting that the structure formation of the system occurs in the W_c range over ca. 0.6 (g/g) with the presence of freezing bound water, as observed in the other polyelectrolyte systems.

The foregoing observations indicate that various kinds of polyelectrolytes, such as lithium, sodium, potassium, magnesium and calcium salts of carboxymethylcellulose, sodium cellulose sulphate, lithium, sodium, potassium and calcium salts of xanthan, and other polyelctrolytes, such as sodium polystyrene sulphonate, form a liquid-crystal phase with an appropriate amount of water. The amount of water which enables these polyelectrolytes to form the liquid-crystal phase is in the W_c range from ca. 0.5 to ca. 3.0. (g/g), depending on the kind of polyelectrolyte. It has also been shown that bound water in the water–polyelectrolyte systems plays an important role in the formation of liquid-crystal phase. The NMR study has shown that water in the system is in a state ranging from non-rigid solid to viscous liquid and that the motion of counter ions in the system is profoundly influenced by the molecular motion of water.

5. Conclusions

Crucial role of water molecules restrained in hydrophilic polymers has been suggested. The relationship between water, higher order structure formation and thermal properties will lead to a more enhanced understanding of the nature of hydrophilic polymers.

References

[1] T. Hatakeyama, F.X. Quinn, in: Thermal Analysis, Fundamentals and Applications to Polymer Science, John Wiley, New York, 1994, Chap. 2.
[2] T. Hatakeyama, K. Nakamura, H. Hatakeyama, Thermochim. Acta 123 (1988) 153.
[3] S. Nakamura, M. Todoki, K. Nakamura, H. Kanetsuna, Thermochim. Acta 136 (1988) 163.
[4] T. Hatakeyama, H. Kanetsuna, Thermochim. Acta 146 (1989) 327.

[5] See, e.g., S. Yano, H. Hatakeyama, T. Hakeyama, in: C. Schuerch (Ed.), Cellulose and Wood, John Wiley and Sons, New York, 1989, p. 389.
[6] H. Maeda, in: N. Maeno, T. Hondah (Eds.), Physics and Chemistry of Ice, Hokkaido University Press, Sapporo (1992), p. 254.
[7] A. Bizet, N. Nakamura, Y. Teramoto, T. Hatakeyama, Thermochim. Acta 237 (1994) 147.
[8] A. Bizet, N. Nakamura, Y. Teramoto, T. Hatakeyama, Thermochim. Acta 241 (1994) 191.
[9] I. Hatta, T. Atake, Netsu Sokutei 16 (1989) 10.
[10] I. Hatta, A.J. Ikushima, Jpn. J. Appl. Phys. 20 (1981) 1995.
[11] F.C. Magne, H.J. Portas, H.A. Wakeham, J. Amer. Chem. Soc. 69 (1947) 1896.
[12] F.C. Magne, E.L. Skau, Textile Res. J. 22 (1952) 748.
[13] J.E. Ayer, J. Polym. Sci. 21 (1956) 455.
[14] M.F. Froix, R.A. Nelson, Macromol. 8 (1975) 726.
[15] R.A. Nelson, J. Appl. Polym. Sci. 21 (1977) 645.
[16] K. Nakamura, T. Hatakeyama, H. Hatakeyama, Textile Res. J. 51 (1981) 607.
[17] L. Salmen, in: C.F. Baker (Ed.), Transactions of the Tenth Fundamental Research Symposium, Oxford, 1993, p. 369.
[18] D. Eisenberg, W. Kauzman, The Structure and Properties of Water, Oxford University Press, London, 1969, p. 93.
[19] H. Hatakeyama, T. Hatakeyama, Makromol. Chem. 182 (1981) 1655.
[20] F. Horii, A. Hirai, R. Kitamaru, in: J.C. Arthur (Ed.), Polymers and Elastomers, ACS Symposium Series No. 260 ACS, Washington D.C., 1984, p. 27.
[21] T. Hatakeyama, H. Hatakeyama, in: J.F. Kennedy, G.O. Phillips, D.J. Wedlock, P.A. Williams (Eds.), Cellulose and its Derivatives, Ellis Horwood, Chichester, 1985, p. 87.
[22] H. Hatakeyama, T. Hatakeyama, J. Nakamura, J. Appl. Polym. Sci. Appl. Polym. Symp. 37 (1983) 979.
[23] K. Nakamura, T. Hatakeyama, H. Hatakeyama, Polymer 24 (1983) 871.
[24] T. Hatakeyama, Y. Ikeda, H. Hatakeyama, in: J.F. Kennedy, G.O. Phillips, P.A. Williams (Eds.), Wood and Cellulosics, Ellis Horwood, Chichester (1987), p. 23.
[25] T. Hatakeyama, Y. Ikeda, H. Hatakeyama, Makromol. Chem. 118 (1987) 1875.
[26] T. Hatakeyama, in: J.F. Kennedy, G.O. Philips, P.A. Williams (Eds.), Cellulose: Structural and Functional Aspects, Ellis Horwood, Ltd., Chichester, 1989, p. 45.
[27] K. Nakamura, T. Hatakeyama, H. Hatakeyama, Text. Res. J. 53 (1983) 682.
[28] T. Hatakeyama, S. Hirose, H. Hatakeyama, Makromol. Chem. 184 (1983) 1265.
[29] W. Whitney, R.P. Andrews, Polym. Sci., C 16 (1967) 2981.
[30] T. Hatakeyama, K. Nakamura, H. Hatakeyama, Polymer 19 (1978) 593.
[31] T. Hatakeyama, H. Hatakeyama, Sen-i Gakkaishi (J. Soc. Fiber Sci. Technol.), 39 (1983) T-461.
[32] S.M. Wofpert, A. Weistz, B. Wunderlich, J. Polym. Sci., A 2(9) (1971) 1887.
[33] H. Yoshida, K. Nakamura, Y. Kobayashi, Polym. J. 14 (1982) 855.
[34] T. Hatakeyama, K. Kanetsuna, Kobunshi Kagaku (J. Polym. Chem.) 25 (1968) 431.
[35] W.M. Prest Jr., F.B. Roberts Jr., Annals of the New York Academy of Sciences 371 (1981) 67.
[36] A. Suggett, in: F. Franks (Ed.), Water, A Comprehensive Treatise, Vol. 4, Chap. 6, p. 519.
[37] G.O. Phillips, in: W. Glasser, H. Hatakeyama (Eds.), Viscoelasticity of Biomaterials, ACS Symp. Ser. 489, Amer. Chem. Soc., Wahington D.C., 1992, p. 168.
[38] E.A. Balazs (Ed.), Chemistry and Molecular Biology of the Intercellular Matrix, Vols. 1 and 2, Academic Press, 1970.
[39] E.R. Morris, D.A. Rees, E.J. Welsh, J. Mol. Biol. 138 (1980) 375; E.R. Morris, D.A. Rees, E.J. Welsh, J. Mol. Biol. 138 (1980) 383.
[40] E.R. Morris, D.A. Rees, E.J. Welsh, Carbohydrate Polymers 10 (1981) 5.
[41] R.H. Pearce, B.J. Grimmer, in: W. Montgna, J.P. Bentrly, R.L. Dobson (Eds.), Advances in the Biology of Skin, II, Appleton, NY, 1970, p. 89.
[42] D.J. Wedlock, G.O. Phillips, A. Davis, J. Gormally, W. Wyn-Jones, Int. J. Biol. Macromol. 5 (1983) 186.
[43] H. Yoshida, T. Hatakeyama, H. Hatakeyama, Kobunnshi Ronnbunnshu 46 (1989) 597.
[44] S. Takigami, M. Takgami, G.O. Phillips, Carohydrate Polymers 22 (1993) 153.
[45] T. Hatakeyama, H. Yoshida, K. Nakamura, H. Hatakeyama, in: N. Maeno, T. Hondah (Eds.), Physics and Chemistry of Ice, Hokkaido University Press, Sapporo, 1992, p. 262.
[46] H. Yoshida, T. Hatakeyama, H. Hatakeyama, in: W. Glasser, H. Hatakeyama (Eds.), Viscoelasticity of Biomaterials, ACS Symp. Ser., 489, Amer. Chem. Soc., Wahington D.C., 1992, p. 385.
[47] T. Hatakeyama, H. Hatakeyama, Koubunshi Ronbunshu (J. of High Polymers), 1996, in press.
[48] H. Yoshida, T. Hatakeyama, H. Hatakeyama, in: N. Maeno, T. Hondah (Eds.), Physics and Chemistry of Ice, Hokkaido University Press, 1992, p. 282.
[49] G.R. Sanderson, R.C. Clark, Food Technol. 4 (1983) 63.
[50] R. Chandrasekaran, L.C. Puigjaner, K.L. Joyce, S. Arnott, Carbohydrate Res. 181 (1988) 23.
[51] M. Tako, A. Sakae, S. Nakamura, Agric. Bio. Chem. 53 (1989) 771.
[52] R. Chandrasekaran, V.G. Thailamba, Carbohydrate Polymers 12 (1990) 431.
[53] F.X. Quinn, T. Hatakeyama, H. Yoshida, M. Takahashi, H. Hatakeyama, Polymer Gels and Networks 1 (1993) 93.
[54] Food Hydrocolloids, Special Issue of Gelllan, 7 (1993) 50.
[55] T. Hatakeyama, F.X. Quinn, H. Hatakeyama, Carbohydate Polymers 30 (1996) 155.
[56] M. Watase, K. Nishinari, Food Hydrocolloids 7 (1993) 449.
[57] R.L. Davidson (Ed.), Handbook of Water-soluble Gums and Resins, McGraw-Hill, New York, 1980.
[58] K. Okuyama, S. Arnott, R. Moorhouse, M.D. Walkinshaw, E.D. T. Atkins, C. Wolf-Ullish, in: A.D. Fresh, K.H. Gardener (Eds.), Fiber Diffraction Methods, Amer. Chem. Soc., Washington, DC., 1980, p. 411.

[59] J.G. Southwick, A.M. Jamieson, J. Blackwell, Macromol. 14 (1981) 1728.
[60] G. Maret, M. Milas, M. Rinaudo, Polym. Bull. 4 (1981) 291.
[61] H. Yoshida, T. Hatakeyama, H. Hatakeyama, Polymer 31 (1990) 693.
[62] T. Sato, T. Norisuye, H. Fujita, Polym. J. 16 (1984) 341.
[63] S.B. Ross-Murphy, V.J. Morris, E.R. Morris, Faraday Symp. Chem. Soc. 18 (1983) 115.
[64] F.X. Quinn, T. Hatakeyama, M. Takahashi, H. Hatakeyama, Polymer 35 (1994) 1248.
[65] K. Nishinari, T. Takaya, M. Watase, K. Kohyam, H. Iida, in: P.O. Williams, G.O. Phillips (Eds.), Gum and Stabilizers for the Food Industry, 1994, p. 359.
[66] K. Nishinari, T. Takaya, M. Watese, in: K. Nishinari, E. Doi (Eds.), Food Hydrogcolloids: Structure, Properties and Functions, Plenum Press, New York, 1994, p. 473.
[67] K. Nishinari, M. Watase, Themochim. Acta 206 (1992) 149; K. Nishinari, P.A. Williams, G.O. Phillips, Food Hydrocolloids 6 (1992) 199.
[68] R. Tanaka, T. Hatakeyama, H. Hatakeyama, Food Hydrocolloids, in press.
[69] S. Takgami, M. Takigami, G.O. Phyllips, Carbohydrate Polymers 26 (1995) 11; S. Takgami, M. Takigami, G.O. Phillips, Food Hydrocolloids 10 (1996) 11.
[70] T. Hatakeyama, H. Hatakeyama, K. Nakramura, Thermochim. Acta 253 (1995) 137.
[71] K. Nakamura, T. Hatakeyama, H. Hatakeyama, Thermochim. Acta 267 (1995) 343.
[72] P.J. Flory, Principles of Polymer Chemistry, Cornell University Press, Ithaca, 1959.
[73] T. Hatakeyama, A. Yamauchi, H. Hatakeyama, Eur. Polym. J. 20 (1984) 61.
[74] M. Nagura, T. Hamano, H. Ishikawa, Polymer 30 (1989) 762.
[75] M. Watase, Chem. Soc. Japan 9 (1983) 1254.
[76] V.I. Lozinsky, E.V. Solodova, A.L. Zubov, I.W. Simenel, J. Appl. Polym. Sci 58 (1995) 171.
[77] T. Hatakeyama, A. Yamauchi, H. Hatakeyama, Eur. Polym. J. 23 (1984) 361.
[78] W.J. MacKnight, W.P. Taggart, R.S. Stein, J. Polym. Sci. Symp. 45 (1974) 113.
[79] N. Ise, T. Okubo, K. Yamamoto, H. Kawai, T. Hashimoto, M. Fujimura, H. Hirai, J. Amer. Chem. Soc. 102 (1980) 7901.
[80] S.B. Ross-Murphy, V.J. Morris, E.R. Morris, Faraday Symp. Chem. Soc. 18 (1983) 115.
[81] N. Ise, T. Okubo, K. Yamamoto, H. Matsuoka, H. Kawai, T. Hashimoto, M. Fujimura, J. Chem. Phys. 78 (1983) 541.
[82] N. Ise, Angew, Chem. (Intl. Ed. Eng.) 25 (1986) 323.
[83] N. Ise, H. Matsuoka, K. Ito, Macromol. 22 (1989) 1.
[84] H. Hatakeyama, H. Yoshida, T. Hatakeyama, in: J.F. Kennedy, G.O. Phillips, D.J. Williams (Eds.), Cellulose and its Derivatives, Ellis Horwood, Chichester, 1985, p. 255.
[85] T. Hatakeyama, K. Nakamura, H. Yoshida, H. Hatakeyama, Thermochim. Acta 88 (1985) 223.
[86] H. Hatakeyama, H. Iwata, T. Hatakeyama, in: J.F. Kennedy, G.O. Phillips, P.A. Williams (Eds.), Wood and Cellulosics, Ellis Horwood, Chichester, 1987, p. 39.
[87] K. Nakamura, T. Hatakeyama, H. Hatakeyama, in: J.F. Kennedy, G.O. Phillips, P.A. Williams (Eds.), Wood Cellulosics, Ellis Horwood, Chichester, 1987, p. 97.
[88] T. Hatakeyama, H. Yoshida, H. Hatakeyama, Polymer 28 (1987) 1282.
[89] H. Hatakeyama, K. Nakamura, T. Hatakeyama, in: C. Schuerch (Ed.), Cellulose and Wood – Chemistry and Technology, John Wiley & Sons, New York, 1989, p. 419.
[90] T. Hatakeyama, S. Yamamoto, S. Hirose, H. Hatakeyama, in: C. Schuerch (Ed.), Cellulose and Wood – Chemistry and Technology, John Wiley & Sons, New York, 1989, p. 431.
[91] H. Hatakeyama, T. Hatakeyama, in: J.F. Kennedy, G.O. Phillips, P.A. Williams (Eds.), Cellulose – Structural and Functional Aspects, Ellis Horwood, Chichester, 1989, p. 131.
[92] H. Yoshida, T. Hatakeyama, H. Hatakeyama, in: J.F. Kennedy, G.O. Phillips, P.A. Williams (Eds.), Cellulose – Structural and Functional Aspects, Ellis Horwood, Chichester, 1989, p. 305.
[93] H. Hatakeyama, Kagaku to Kogyo (Chemistry and Chemical Industry) 42 (1989) 878.
[94] T. Hatakeyama, H. Hatakeyama, Poly. Adv. Tech. 1 (1990) 305.
[95] H. Hatakeyama, T. Hatakeyama, in: L. Salmen, M. Htun (Eds.), Properties of Ionic Polymer – Natural and Synthetic, STFI Series A-989, Stockholm, 1991, p. 123.
[96] T. Hatakeyama, N. Bahar, H. Hatakeyama, Sen-i Gakkaishi 47 (1991) 417.
[97] K. Nakamura, T. Hatakeyama, H. Hatakeyama, Polym. J. 23 (1991) 253.
[98] T. Hatakeyama, H. Hatakeyama, in: W.G. Glasser, H. Hatakeyama (Eds.), Viscoelasticity of Biomaterials, ACS Symp. Ser. 489 (1992), p. 329.
[99] T. Hatakeyama, H. Hatakeyama, in: J.F. Kennedy, G.O. Phillips, P.A. Williams (Eds.), Cellulosics: Chemical, Biochemical and Material Aspects, Ellis Horwood, Chichester, 1993, p. 225.
[100] K. Nakamura, T. Hatakeyama, H. Hatakeyama, in: J.F. Kennedy, G.O. Phillips, P.A. Williams {Eds.), Cellulosics: Chemical, Biochemical and Materials Aspects, Ellis Horwood, Chichester, 1993, p. 243.